ChemComm

COMMUNICATION

View Article Online
View Journal | View Issue

Cite this: *Chem. Commun.*, 2025, **61**, 3700

Received 23rd November 2024,
Accepted 3rd February 2025

DOI: 10.1039/d4cc06224h

rsc.li/chemcomm

Molten salt-mediated electrosynthesis of MoS_2 nanosheet-supported Rh nanoclusters for highly efficient electrocatalytic hydrogen evolution†

Qing Yan, [ab] Yuhui Liu, *[e] Yang Zhao,*[d] Xiangqian Zhou[a] and Weiyong Yuan *[bc]

We report the synthesis of MoS_2 nanosheet-supported Rh nanoclusters *via* a facile yet efficient molten salt electrolysis method followed by wet chemical reduction for electrocatalytic hydrogen evolution. In-depth study reveals that the uniform Rh nanoclusters on MoS_2 nanosheets can shorten the electronic transport path, and effectively promote the hydrogen evolution reaction kinetics.

With the continuous development of wind and solar power generation, the use of green electricity to produce hydrogen has become a research hotspot. Electrolysis of water splitting is an effective method for high-purity hydrogen production.[1–3] However, this process consumes excessive energy due to the slow hydrogen evolution reaction (HER) kinetics.[4–7] Therefore, there is an urgent need to discover cathode catalysts with low overpotential and high activity in generating hydrogen. Platinum is currently recognized as the optimal choice for HER catalysis under acidic conditions. However, the limited reserves and high price hinder its widespread applications. Additionally, acidic conditions are more favorable for the HER compared to neutral and alkaline ones.[8–10] Unfortunately, most transition metals are not stable under acidic conditions. Consequently, much effort has been devoted to designing affordable and stable cathode catalysts that can perform well under alkaline or neutral conditions.

Molybdenum disulfide (MoS_2) is promising as a HER catalyst due to their advantages such as tunability, low cost, and chemical stability.[11–14] However, the catalytic performance of pristine molybdenum disulfide is not satisfactory mainly because of in-plane inertness and limited edge active sites.[15] Therefore, various strategies have been developed to enhance its catalytic activity. In particular, the decoration of MoS_2 nanosheets with HER-active components holds great promise since this approach could not only restrict the restacking between nanosheets, but greatly increase the number of exposed active sites. Rhodium (Rh) could serve as an ideal candidate of the active components to modify MoS_2 nanosheets because of its HER activity like that of Pt and much higher corrosion resistance under harsh alkaline/acidic conditions than that of Pt. Currently, there are still great challenges to fabricate the hybrids of Rh-modified MoS_2 nanosheets for high-performance and low-cost HER catalysis: the synthesis techniques for MoS_2 nanosheets, including the hydrothermal method and chemical vapor deposition, frequently exhibit low production yields, require long time, and are carried out in closed reaction systems, and thus it is crucial to explore high-throughput methods for producing MoS_2 nanosheets; in addition, Rh is expensive and scarce in nature, and it is therefore essential to significantly improve its utilization for greatly enhancing the activity of MoS_2 nanosheets, while reducing its loading.

The molten salt electrolysis could be a highly promising environment-friendly strategy to rapidly synthesize MoS_2 nanosheets with high product yields.[16] The high-temperature environment can further greatly accelerate the chemical reaction rate and thereby enhance the synthesis efficiency. Rh in the form of nanoclusters could significantly increase its dispersion and facilitate its interfacial charge transfer through the Rh/MoS_2 interfaces;[17] therefore, employing Rh nanoclusters to decorate the MoS_2 nanosheets may effectively improve the catalytic activity with extremely low precious metal content. In this study, for the first time, we synthesized MoS_2 nanosheet-supported Rh nanoclusters (MoS_2 NS@Rh NC) *via* the facile yet efficient molten salt electrolysis method for application as an

[a] *School of Biological and Chemical Engineering, NingboTech University, Ningbo 315100, P. R. China*
[b] *Ningbo Innovation Center, Zhejiang University, Ningbo, 315100, China. E-mail: wyyuan@zju.edu.cn*
[c] *College of Chemical & Biological Engineering, Zhejiang University, Hangzhou 310027, P. R. China*
[d] *College of Water Conservancy and Hydropower Engineering, Sichuan Agricultural University, Ya'an 625014, China. E-mail: yangzhao@sicau.edu.cn*
[e] *East China University of Technology, Nanchang 30013, China. E-mail: liuyuhui@ecut.edu.cn*

† Electronic supplementary information (ESI) available: Experimental section; XRD and TEM of the MoS_2 NS sample; TEM, XRD, and XPS of the MoS_2 NS@Rh NC and so on. See DOI: https://doi.org/10.1039/d4cc06224h

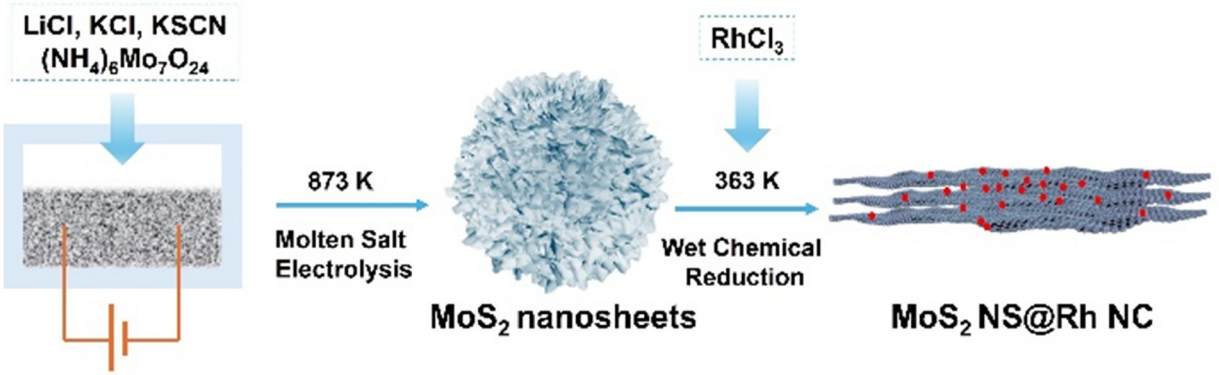

Fig. 1 Schematic illustration of the synthesis of MoS_2 NS@Rh NC.

electrocatalyst toward the HER. It is discovered that the uniform Rh nanoclusters on the MoS_2 nanosheets obtained using 3.5% Rh can effectively promote the HER. This catalyst exhibits a small overpotential of 27 mV at 10 mA cm^{-2}, which is close to that of commercial Pt/C (12 mV). In addition, it shows a small Tafel slope of 47 mV dec^{-1} with good stability.

The synthesis process of MoS_2 NS@Rh NC is schematically shown in Fig. 1. LiCl, KCl, anhydrous $(NH_4)_6Mo_7O_{24}$, and anhydrous KSCN were directly introduced into the reactor. The electrolysis was then carried out at a temperature of 873 K with a current density of 1.55 A cm^{-2} for only 1 h. The black precipitate obtained was rinsed thoroughly with distilled water and anhydrous ethanol multiple times. An appropriate volume of $RhCl_3$ solution (1 mg mL^{-1}) was subsequently added into the suspension and this reaction system was maintained at 363 K for 30 min.

The XRD pattern of MoS_2 NS@Rh NC (Fig. 2A) shows characteristic peaks at 14.4°, 32.7°, 33.5°, 35.9°, 39.6°, 49.8°, 58.4°, and 60.4°, which correspond to (002), (100), (101), (102), (103), (105), (110), and (112) planes of hexagonal MoS_2 (ICCD#01-077-1716; space group, *P*63; $a_0 = b_0 = 3.1602$ Å; $c_0 = 12.2940$ Å). There is no peak from Rh, which could be due to the too low content of Rh in the sample MoS_2 NS@Rh NC. The peaks for the high-resolution XPS spectrum of MoS_2 NS@Rh NC were deconvoluted by referring to previous literature.[18] The Rh 3d can be deconvoluted into peaks at 308.2, 309.2, and 313.2 eV, which are ascribed to Rh^{1+}, Rh^{2+} $3d_{5/2}$, and Rh^{2+} $3d_{3/2}$, respectively.[19] The high-resolution XPS spectrum of Mo 3d shows Mo^{4+} signals located at 229.8 and 233.2 eV of Mo $3d_{5/2}$ and Mo $3d_{3/2}$, accompanied by the relatively weak Mo^{6+} signals of 236.9 and 233.9 eV arising from the surface oxidation of MoS_2 nanosheets.[17] The peak at 226.9 eV belongs to S 2s. Fig. 2D shows three peaks at 162.6 eV 163.8 eV and 169.7 eV, which can be assigned to S $2p_{3/2}$ and S $2p_{1/2}$ of S^{2-} and the S species in MoS_2.[20,21]

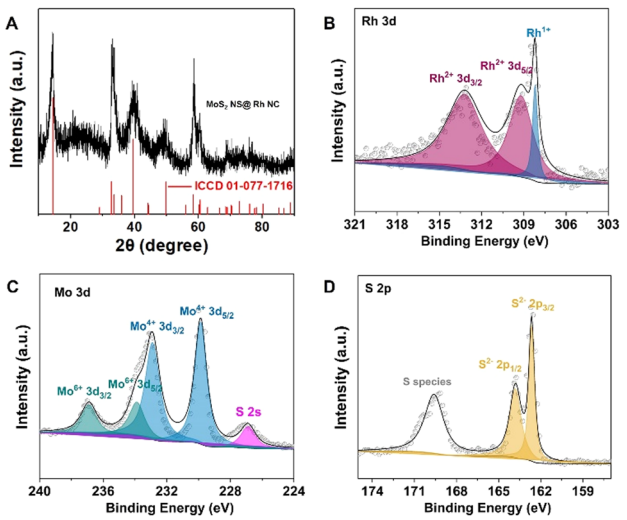

Fig. 2 The XRD image of MoS_2 NS@Rh NC (A) and XPS spectra of Rh 3d (B), Mo 3d (C), and S 2p (D).

The scanning electron microscopy (SEM) image of MoS_2 NS@Rh NC (Fig. 3A) shows a flower-like nanostructure assembled from interconnected nano-flakes. The SEM-EDX elemental mapping images of MoS_2 NS@Rh NC (Fig. 3B) clearly indicate that the Mo (red color), S (green color), and Rh (blue color) elements are distributed homogeneously in Rh-MoS_2. The transmission electron microscopy (TEM) image further indicates that the MoS_2 NS@Rh NC exhibits a typical nanosheet structure, which is beneficial for its contact with the electrolyte. The high-magnification TEM image (Fig. 3D) reveals that Rh nanoclusters are evenly distributed on the surface of the MoS_2 nanosheets. The TEM images for the samples of 7.0% MoS_2 NS@Rh NC and 2.8% MoS_2 NS@Rh NC are displayed in Fig. S2 (ESI†). It shows that the Rh nanocluster's size and the intensity of the dispersion of 7.0% MoS_2 NS@Rh NC are larger than that of 2.8% MoS_2 NS@Rh NC. The high-resolution transmission electron microscopy (HRTEM) image (Fig. 3E) shows clear lattice fringes with a spacing of 0.61 nm, which corresponds to the (002) plane of hexagonal MoS_2. The crystalline fringes can be observed with the lattice spacing of 0.23 nm (Fig. S4, ESI†), which can be assigned to the (103) plane. Fig. S5 (ESI†) shows the adsorption–desorption and pore size distribution curves. The sample has a BET surface area of 173.23 m^2 g^{-1} with the average pore diameter of 9.69 nm, which offers rich space for the adsorption of water molecules and desorption of hydrogen molecules.

The standard three-electrode system was employed to evaluate the HER performance of the MoS_2 NS@Rh NC electrode.

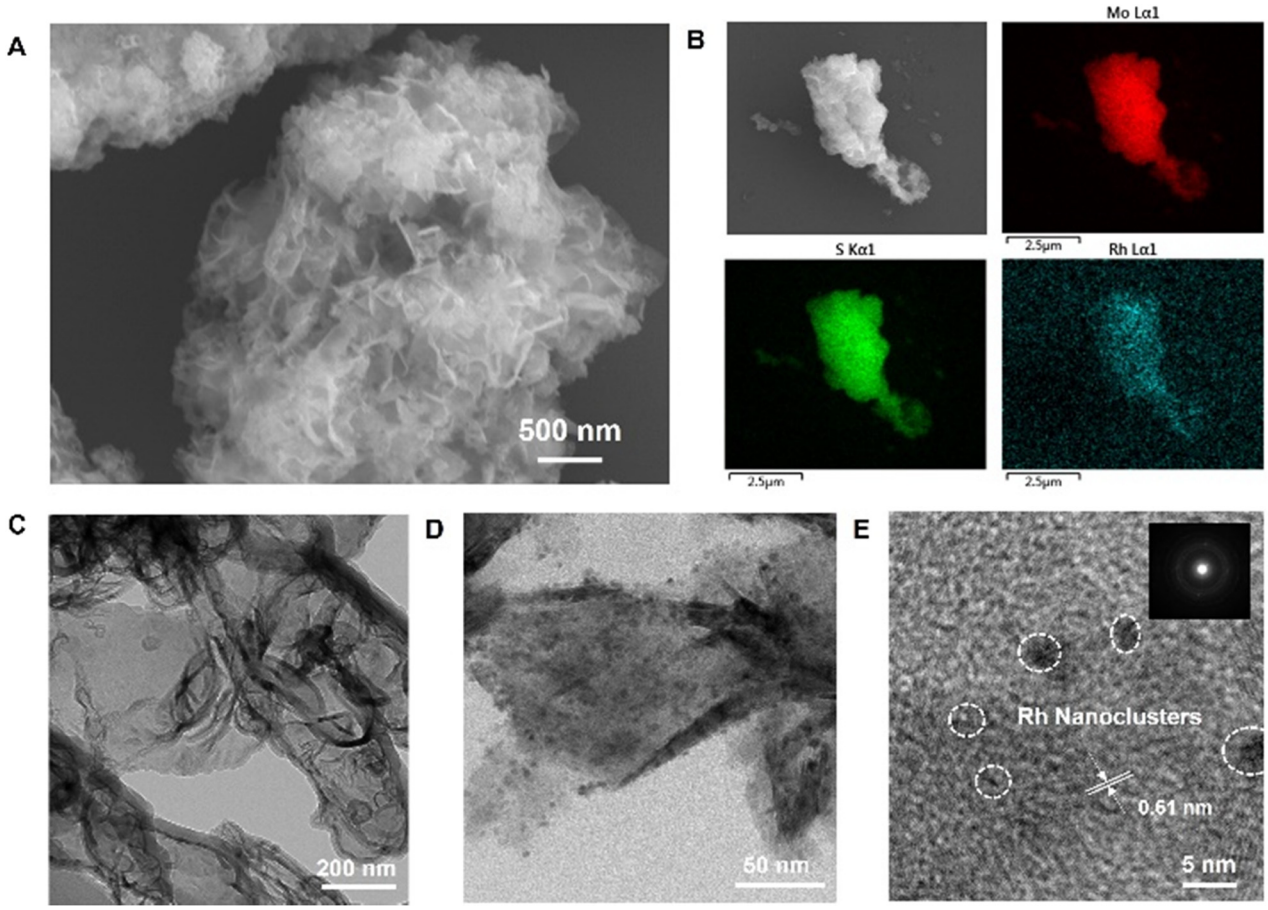

Fig. 3 SEM image of MoS_2 NS@Rh NC (A), energy-dispersive X-ray (EDX) results (B), and TEM (C and D) and HRTEM (E) images of MoS_2 NS@Rh NC.

The LSV curves (Fig. 4A) show that the 3.5 wt% MoS_2 NS@Rh NC electrode has a small overpotential of 27 mV at 10 mA cm^{-2}, which is smaller than that of MoS_2 (308 mV), and close to the catalyst of 20% Pt/C (12 mV). The Tafel slope is an important evaluation index for the catalytic reaction kinetics. The Tafel plots (Fig. 4B) show that the Tafel slope of 3.5 wt% MoS_2 NS@Rh NC (47 mV dec^{-1}) is close to that of 20% Pt/C (36 mV dec^{-1}), and much smaller than that of MoS_2 (142 mV dec^{-1}).

The Tafel slope values of the above samples indicate that the introduction of Rh nanoclusters can effectively enhance the HER kinetics of MoS_2, because the uniform dispersion of Rh can provide a more convenient channel for electron transfer. In addition, the content of Rh has been tailored for investigating the influence of Rh content on HER performance. As shown in Fig. 4C, with the increase in the Rh content, the HER performance of the catalyst is improved significantly. When the content of Rh reaches 3.5%, the HER performance is close to that when the content is 7.0%. Therefore, the content of 3.5% Rh is the ideal content. The Tafel slope (Fig. 4D) further indicates that the reaction kinetics of the 3.5% MoS_2 NS@Rh NC electrode is very similar to that of 7.0% MoS_2 NS@Rh NC. Electrochemical impedance spectroscopy (EIS) was further employed to explore the HER kinetics. The EIS data (Fig. 4E) show that the 3.5% MoS_2 NS@Rh NC electrode has the smallest electron transfer resistance, indicating the fastest HER on the surface of 3.5% MoS_2 NS@Rh NC. Stability is another important factor in evaluating catalysts. The chronopotentiometric curve of the 3.5% MoS_2 NS@Rh NC electrode at 10 mA cm^{-2} (Fig. 4F) shows negligible change in the potential, indicating its good stability. For further evaluation of morphology stability, TEM (Fig. S6, ESI†) analysis was performed on the sample after stability testing. It was found that the test pieces still maintained their original nanosheets with a dispersed nanocluster structure after the stability testing, exhibiting good morphology stability. The XRD (Fig. S7, ESI†) stability testing shows that the 3.5% MoS_2 NS@Rh NC retains the stable phase structure. In addition, the XPS (Fig. S8, ESI†) after stability testing indicates that the Rh^{2+}, Mo^{6+}, and S^0 species almost disappear, which indicates that the valences of the catalysts have changed during the electroreduction process.

The superior HER performance of MoS_2 NS@Rh NC could be ascribed to the following reasons: first, the 3D interconnected nanosheet structure offers numerous exposed active sites for adsorption of water molecules and desorption of hydrogen molecules; second, the Rh nanoclusters uniformly assembled on the surface of MoS_2 nanosheets shorten the electron transport paths and enhances the intrinsic activity, leading to enhanced reaction kinetics; third, the highly active

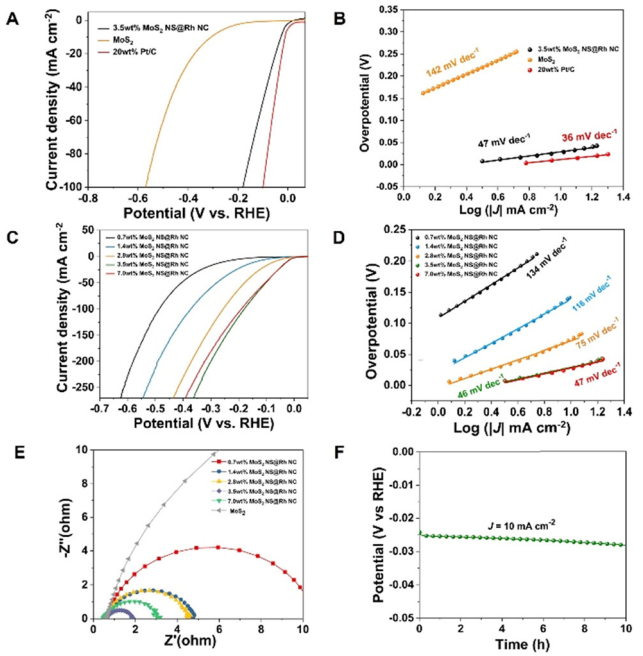

Fig. 4 LSV curves (A) and Tafel plots (B) of different samples. LSV curves (C) and Tafel plots (D) of MoS_2 NS@Rh NC with different Rh contents. Nyquist plots (E) of MoS_2 NS@Rh NC with different Rh contents. The chronopotentiometry (CP) image (F) of MoS_2 NS@Rh NC for 10 hours.

Rh nanoclusters anchored on the planes of the MoS_2 nanosheets significantly enhance the in-plane HER activity.

In summary, MoS_2 nanosheet-supported Rh nanoclusters were synthesized *via* a facile, yet efficient molten salt electrolysis method followed by wet chemical reduction, which can be easily implemented for large-scale synthesis. The uniform Rh nanoclusters on MoS_2 nanosheets can enhance the intrinsic activity of the catalysts, as well shorten the electron transport path, and effectively promote the HER kinetics. This study not only creates a highly efficient and inexpensive HER catalyst for water splitting but provides a novel strategy to synthesize unique nanostructured materials for important applications such as catalysis, energy storage, the environment, and biomedicine.

This work was financially supported by "Science and technology innovation Yongjiang 2035" key technology breakthrough plan (Grant No. 2024Z203), the Scientific Research Fund of Zhejiang Provincial Education Department (Grant No. Y202454727), the Natural Science Foundation of Sichuan Province (Grant No. 2023NSFSC1068), the Yongjiang Talent Introduction Programme (Grant No. 2021A-155-G), Natural Science Foundation of Ningbo, China (Grant No. 2022J156), and Research Fund of Ningbo Innovation Centre, Zhejiang University (Grant No. 704004J20240524).

Data availability

The data supporting this article have been included as part of the ESI.†

Conflicts of interest

The authors declare no competing financial interest.

References

1 W. Hu, Q. Yan, X. Wang, J. Lu, Q. He, Q. Zhang and W. Yuan, *Adv. Funct. Mater.*, 2024, 2411904.
2 X. Liu, B. Li, F. A. Soto, X. Li, R. R. Unocic, P. B. Balbuena, A. R. Harutyunyan, J. Hone and D. V. Esposito, *ACS Catal.*, 2021, **11**, 12159–12169.
3 W. Han, J. Ning, Y. Long, J. Qiu, W. Jiang, Y. Wang, L. A. Shah, D. Yang, A. Dong and T. Li, *Adv. Energy Mater.*, 2023, **13**, 2300145.
4 H. Xiong, X. Zhang, X. Peng, D. Liu, Y. Han and F. Xu, *Chem. Commun.*, 2024, **60**, 11112–11115.
5 Y. Li, J. Han, W. Bao, J. Zhang, T. Ai, M. Yang, C. Yang and P. Zhang, *J. Energy Chem.*, 2024, **90**, 590–599.
6 L. A. Zavala, K. Kumar, V. Martin, F. Maillard, F. Maugé, X. Portier, L. Oliviero and L. Dubau, *ACS Catal.*, 2023, **13**, 1221–1229.
7 S. Qiang, Z. Li, S. He, H. Zhou, Y. Zhang, X. Cao, A. Yuan, J. Zou, J. Wu and Y. Qiao, *Nano Energy*, 2025, **134**, 110564.
8 X. Guo, E. Song, W. Zhao, S. Xu, W. Zhao, Y. Lei, Y. Fang, J. Liu and F. Huang, *Nat. Commun.*, 2022, **13**, 5954.
9 Y. Wang, W. Luo, S. Gong, L. Luo, Y. Li, Y. Zhao and Z. Li, *Adv. Mater.*, 2023, **35**, 2302499.
10 Y. Zhang, Z. Li, S. He, Y. Qiao, A. Yuan, J. Wu and H. Zhou, *J. Colloid Interface Sci.*, 2025, **679**, 20–29.
11 R. Li, J. Liang, T. Li, L. Yue, Q. Liu, Y. Luo, M. S. Hamdy, Y. Sun and X. Sun, *Chem. Commun.*, 2022, **58**, 2259–2278.
12 J. Xu, A. Gulzar, Y. Liu, H. Bi, S. Gai, B. Liu, D. Yang, F. He and P. Yang, *Small*, 2017, **13**, 1701841.
13 S. Ma, Q. Yan, H. Gui, R. Gao, L. Zhang, X. Bai and K. Cheng, *New J. Chem.*, 2025, **49**, 84–91.
14 J. Lim, S. J. Heo, M. Jung, T. Kim, J. Byeon, H. Park, J. E. Jang, J. Hong, J. Moon, S. Pak and S. Cha, *Small*, 2024, **20**, 2402272.
15 Y. Zhang, X. Wang, X. Song and H. Jiang, *Nano Res.*, 2024, **17**, 9507–9517.
16 J. Luo, Q. Qing, Z. Wang, S. Liu, J. Chen and Y. Lu, *Sep. Purif. Technol.*, 2024, **332**, 125829.
17 Y. Cheng, S. Lu, F. Liao, L. Liu, Y. Li and M. Shao, *Adv. Funct. Mater.*, 2017, **27**, 1700359.
18 J. Chen, Y. Zhuang, Y. Qiao, Y. Zhang, A. Yuan and H. Zhou, *Int. J. Miner., Metall. Mater.*, 2025, **32**, 476–487.
19 L. Yang, G. Li, R. Ma, S. Hou, J. Chang, M. Ruan, W. Cai, Z. Jin, W. Xu, G. Wang, J. Ge, C. Liu and W. Xing, *Nano Res.*, 2021, **14**, 2853–2860.
20 X. Meng, C. Ma, L. Jiang, R. Si, X. Meng, Y. Tu, L. Yu, X. Bao and D. Deng, *Angew. Chem., Int. Ed.*, 2020, **59**, 10502–10507.
21 F.-Y. Yu, H. Sun, H.-Q. Tan, Y.-G. Li, S.-T. Lee and Z.-H. Kang, *Chem. Catal.*, 2024, **4**, 101002.